Synthesis free-template highly micro-mesoporous carbon nanosheet as electrode materials for boosting supercapacitor performances

by Rika Taslim

Submission date: 13-Apr-2023 10:46AM (UTC+0700)
Submission ID: 2063155138
File name: 11._Energy_Research,_july2022.pdf (3.49M)
Word count: 10198
Character count: 53209

Received: 1 March 2022 | Revised: 14 July 2022 | Accepted: 15 July 2022

DOI: 10.1002/er.8493

RESEARCH ARTICLE

INTERNATIONAL JOURNAL OF ENERGY RESEARCH WILEY

Synthesis free-template highly micro-mesoporous carbon nanosheet as electrode materials for boosting supercapacitor performances

Erman Taer[1] | **Apriwandi Apriwandi**[1] | **Miftah Ainul Mardiah**[1] | **Awitdrus**[1] | **Rika Taslim**[2]

[1]Department of Physics, Faculty of Mathematic and Natural Sciences, University of Riau, Riau, Indonesia

[2]Department of Industrial Engineering, State Islamic University of Sultan Syarif Kasim Riau, Riau, Indonesia

Correspondence
Erman Taer, Department of Physics, Faculty of Mathematic and Natural Sciences, University of Riau, Riau, Indonesia.
Email: erman.taer@lecturer.unri.ac.id

Funding information
Direktorat Jenderal Pendidikan Tinggi

Summary

Porous carbon 2D nanosheets (CNSs) with micro-mesopores interconnected are indispensable for energy conversion systems and storage applications. Herein, we synthesize free-template highly micro-mesoporous carbon nanosheet as electrode material for boosting supercapacitor performances. The activated carbon nanosheets derived from bio-waste were prepared by chemical impregnation followed by high-temperature pyrolysis without hard/soft/salt template-assisted and free-binder adhesives. Garlic skin wastes were selected as a precursor. Furthermore, activated carbon was designed in pellet/coin solids without the addition of binder materials. The porous carbon pellets exhibit a thin 2D nanosheet structure of 15 nm followed by unique wooden labyrinth-like and rod-like structures. The result showed that the impregnation of different chemical concentrations increases the surface area to 273% as high as 1002.920 $m^2\ g^{-1}$ with a total volume of 1.3270 $cm^3\ g^{-1}$. Moreover, the mesoporosity dominated 66.4%, followed by sub-ultra-micropores. In the symmetric supercapacitor, the carbon nanosheet boosted the specific capacitance almost 3-fold to 320.95 $F\ g^{-1}$ in the aqueous electrolyte of 1 M H_2SO_4. The supercapacitor cell has a high energy density of 43.12 $Wh\ kg^{-1}$ and power density of 161.99 $W\ kg^{-1}$ at a constant current density of 1.0 $A\ g^{-1}$. This work proposes a more effective, green, efficient, and controlled approach to obtain bio-waste-based porous carbon 2D nanosheet with a controlled pore structure for energy conversion and storage systems.

Novelty Statement

The novelty of this study is a green synthesis has possessed highly micro-mesopores nanosheet bio-waste. 2D nanosheet was prepared free-template and free-binder. Sub-ultra-micropores were confirmed with dominated mesoporosity of 66.8%. Carbon nanosheet boosted specific capacitance almost 3-fold to 320.95 $F\ g^{-1}$.

KEYWORDS

bio-waste, electrode materials, nanosheet, sub-ultra-micropores, supercapacitor

1 | INTRODUCTION

The high consumption of fossil fuels by the world's giant industries has been considered a major contributor to climate change, global warming, as well as water, soil, and air pollution. However, dependence on fossil fuels is unavoidable; therefore, it is important to optimize the efficiency of renewable energy sources, conversion, and storage systems. Several studies have been carried out on the development of energy conversion and storage system technologies to optimize the performance of renewable energy sources.[1] Supercapacitors are a type of storage device that provides high energy/power, fast charge/discharge rate, and infinity life cycle compared to batteries and capacitors.[2,3] To certain extent, it has shown an extraordinary specific capacitance of 2395 F g^{-1} with high stability.[4] However, the unbalanced specific energy and power limits further its applications. The electrode material is a key component that aids in the excellent performance enhancement of supercapacitors.[5] They are usually characterized by high surface area,[6] abundantly confirmed sub-ultra-microporous,[7] 3D connected pores,[8] and 200 nm particle sizes[9] indispensable for enhancing its high specific energy. These properties are found in several electrode materials such as graphene/graphene oxide,[10,11] conduction polymers,[12] carbon nanotubes,[13] template-carbon-derived,[14] and porous carbon,[15,16] synthesized by different techniques. Zang et al stated that polym based carbon sources have the potential to produce a high specific surface area of 3270 m^2 g^{-1} with a 3D pore structure made from reduced graphene oxide/polyaniline (rGO/PANI) hybrid film. This superior property enhances specific energy and capacitance of 94 Wh kg^{-1} and 808 F g^{-1}, respectively.[17] Furthermore, Wang et al designed a supercapacitor with a specific energy of 64 Wh kg^{-1} from a metal oxide through in-situ synthesis.[18] In addition, sub-ultra-micropores were confirmed using the porous carbon of bacterial cellulose by means of the KOH impregnation technique, which also showed enhanced electrochemical properties.[7] However, these require highly complex synthesis techniques, expensive and sophisticated specialized equipment, which are considered to be a challenge.

In the past 10 years, nanomaterial technology has been considered one of the strategies to develop energy storage system devices due to its drastically adjustable properties. Furthermore, two-dimensional (2D) nano-sized materials, especially nanosheets, have emerged as an effective approach to enhance energy storage and conversion through increased ion contact area, electrolytic ion diffusion pathways, high electrical conductivity, and hydrophilic properties, which improve performance.[19,20] Peng et al designed a holey carbon nanosheet with a unique structure through self-generated template assistance.[21] In addition, specific energy of 17.92 Wh kg^{-1} with excellent cyclic stability was obtained through nitrogen doping. They claimed that the strategy used is effective for producing nanosheet structures with controlled morphology for supercapacitor applications. Furthermore, lignin-based ultra-thin nanosheet structures were synthesized using a low-cost and environmental NaCl template technique.[22] This study proves that high porosity and ultra-thin sheets are needed for boosting the electrode material performance.[23] A similar study was also carried out by Huo et al, using Iron (III) chloride hexahydrate as the source material.[24] However, techniques including hard, soft, and salt templates are considered ineffective in the synthesis of highly porous 2D nanosheet structures. This is due to its difficulty in obtaining sub-ultra-microporous structures that greatly contribute to the provision of ionic charge contact areas. In addition, their metal residues require corrosive reagents that are toxic and difficult to recycle.

Consequently, porous biomass-based carbon is a suitable raw material to produce a 2D nanosheet which increases the supercapacitor's specific energy due to the unique structure of the biomass basic components of lignocellulose.[25-27] In addition, they also provide a high specific surface area of relatively 3000 m^2 g^{-1}, unique and optimized pore structure, extremely conductive, and good thermal and electrical stability.[28-31] Most importantly, activated carbon synthesized from biomass is relatively easy, simple, inexpensive, abundant, and renewable. Recently, Selvaraj et al carried out research on ways to obtain ultra-high surface area carbon nanosheets from *Prosopis juliflora* wood. The preparation technique is relatively facile, a simple one-step KOH activation resulting in specific energy and capacitance of 32 Wh kg^{-1} and 426 F g^{-1}, respectively.[32] Similar methods and results were also discovered in several other studies that adopted biomass as source material, such as *Moringa oliviera* stem,[33] *Syzygium oleana*,[34] and pineapple leaves.[35] The result obtained in this research tends to be more accurate than the previous studies carried out using the template method. However, the use of adhesive materials such as PVDF, PVA, and PTFE for supercapacitor cell preparation is detrimental to the electrode material's performance, especially its internal resistance.

In this study, micro-mesoporous carbon nanosheets decorated with unique morphological structures were prepared from bio-waste garlic skins using a green technique without templates and adhesives. Zinc chloride was impregnated with three different concentrations followed by high-temperature pyrolysis in N_2 and CO_2 gas environment, selected to convert bio-waste into nanoporous activated carbon. Furthermore, the sample was

designed in the form of a solid pellet by maximizing the self-adhesive nature of the raw material. The morphology confirms the 2D nanosheet decorated with the wooden labyrinth and rod-like structures. In addition, the activated carbon obtained led to an increase in the surface area by 273%, which is relatively as high as 1002.920 m^2 g^{-1}, dominated by 66.4% mesoporosity and confirmed sub-ultra-micropores. Based on the two-electrode configuration system, the supercapacitor cell showed high capacitive properties of 320.95 F g^{-1} at a 1.0 A g^{-1}. Furthermore, in 1 M H_2SO_4 aqueous electrolyte, the specific energy and specific power were 43.12 and 161.99 Wh kg^{-1}, respectively. The results were claimed to be equivalent to other materials, polymers, and graphene oxide as previously described. Finally, this research provides a relatively simple, effective-efficient, and inexpensive approach to produce highly micro-mesoporous carbon 2D nanosheets with enhanced specific energy for high performance and storage systems.

2 | MATERIALS AND METHODS

2.1 | Materials

Garlic skin waste was obtained from the Pekanbaru main market, Indonesia. It was cleaned using DI water and sundried for 48 hours. The skin was further-dried using a vacuum oven at 110°C for 24 hours. The grinding and sifting process was used to convert the dried skin to powder samples with a particle size of <60 μm. Zinc chloride (95%) and sulfuric acid (97%) were extracted from EMD Millipore Corporation and Panreac Quimica Sau. The separator and current collectors used in the fabrication of supercapacitor cells are derived from duck eggshell membranes and stainless steel.

2.2 | Synthesis of highly micro-mesoporous carbon nanosheet

Garlic skin waste-based micro-mesoporous carbon nanosheets were synthesized through a relatively easy approach with zinc chloride impregnation and one-step carbonization-physical activation. A total sample of 30 g was added in a 150 mL zinc chloride solution with different concentrations, including 0.25, 0.50, and 0.75 mol/L. Subsequently, the sample was placed on a hotplate at 80°C for 2 hours. Furthermore, it was dried in an oven to obtain dried-activated carbon powder, which is converted into solid coins/pellets with a diameter of ±19.00 cm without the addition of adhesive (free-binder) by pressing a manual hydraulic press instrument. A total of 20 solid carbon pellets were carbonized and physically activated in the furnace tube. Carbonization was performed from room temperature to 600°C with a gradual increase rate of 1°C/min and 3°C/min in an N_2 gas environment. This was followed by a physical activation process from 600°C to 850°C at 10°C/min in a CO_2 gas environment. Finally, the solid carbon nanosheet samples were neutralized using DI water with the preparatory process shown in Scheme 1. It needs to be noted that the raw material was carbonized and physically activated without zinc chloride impregnation. These were labeled as biochar in all the presented figures and tables.

2.3 | Materials characterization

The porous carbon nanosheets with pellet-free-binder starts with evaluating changes in density during the pyrolysis process by measuring the mass, height, and diameter of the pellet. Density is evaluated using the common formula by assuming that the pellet-free-carbon binder is a tubular geometry. Furthermore, the phase features of the carbon nanosheets were reviewed using the X-ray diffraction method, while the Phillip X-Pert-PW3060/10 instrument and CuKα act as sources. Spacing of XRD interlayer ($d_{002}-d_{100}$) and stack height and stack width (L_c-L_a) were calculated using Bragg's law and the debye-Scherrer equation.[36] The surface morphology was reviewed using scanning electron microscopy, specifically the JEOL-JSM6510LA instrument. In addition, elemental analysis was also evaluated using energy dispersive spectroscopy techniques. Furthermore, Quantachrome-NOVA 1200 instrument was used to confirm specific surface area and pore size distribution in respect to the N_2 gas absorption technique. Specific surface area (S_{BET}) was evaluated using the BET technique (Brunauer-Emmett-Teller), pore size distribution, micropore surface area (S_{micro}), and micropore volume (V_{micro}) further calculated using a technical t-plot and BJH (Barrett-Joyner-Halenda) method.

2.4 | Electrode preparation and electrochemical measurement

A 2-electrode configuration system was used to measure the symmetric supercapacitors' electrochemical behavior. The prototype was prepared in the form of coin layers consisting of two free-binder carbon nanosheet pellets with an active sample of mass 9.8 mg placed in an acrylic cell body, with a size of 2x2cm perforated at a diameter of ±9.0 cm. The carbon nanosheet is placed at the center with a support made of Teflon. Furthermore, a separator

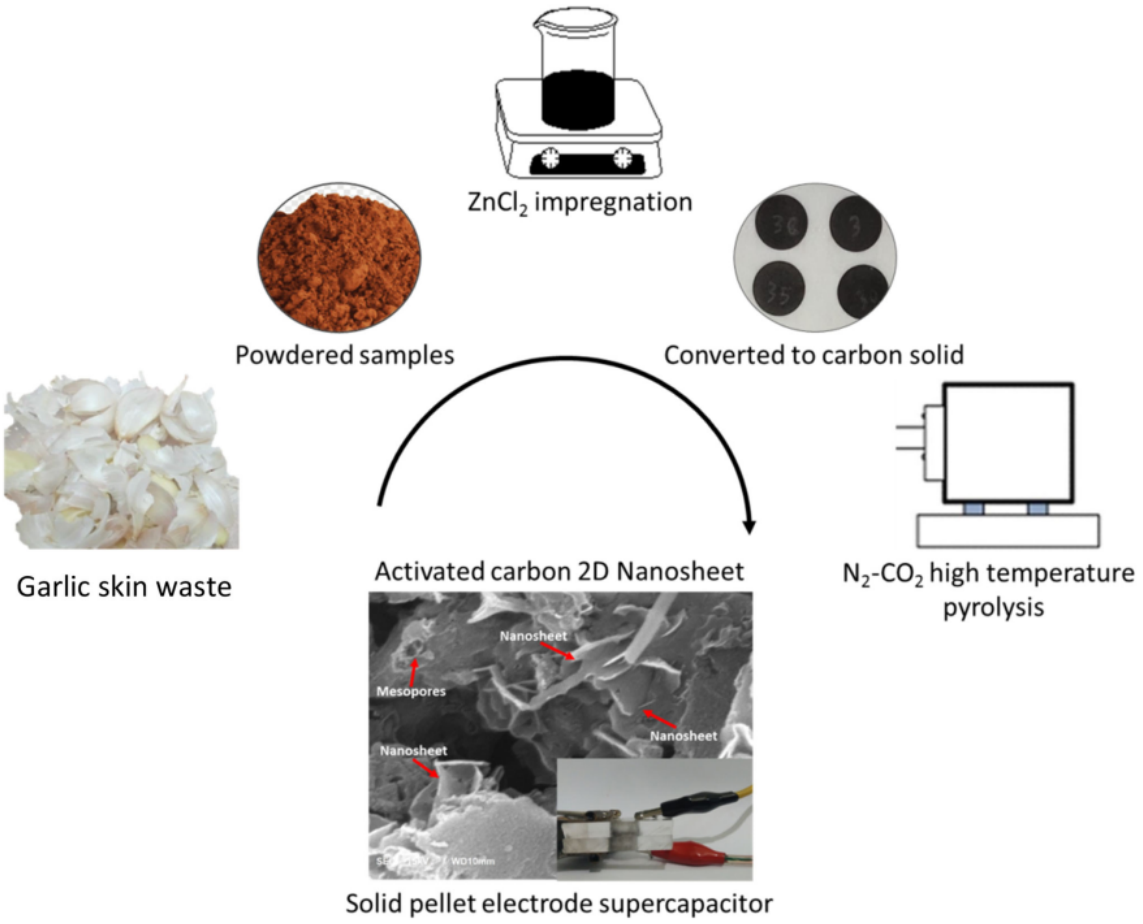

SCHEME 1 Synthesis of highly micro-mesopores carbon nanosheet derived from garlic skin waste

made of organic material from the duck egg membrane was placed between the two electrodes, while stainless steel served as a current collector. The electrochemical properties were confirmed through cyclic voltammetry (CV) and galvanostatic charge-discharge (GCD) techniques. Cyclic voltammetry was reviewed using a Rad-Er 5841 instrument (calibrated with VersaStat II Princeton Applied Research, error ±6.05%) at graded scan rates of 1, 2, 5, 10, and 20 mV s^{-1} with a constant voltage ranging from 0.0 to 1.0 V. The specific capacitance is calculated using the standard equation stated as follows[37]

$$C_{sp} = \frac{1}{s \cdot m \cdot \Delta V} \int iv\, dv$$

C_{sp} is the specific capacitance (F g^{-1}), $\int iv\, dv$ is the integral area of the CV curves, s is the scanning rate (V s^{-1}), ΔV is the operating potential window (V), and m is the mass of activated carbon. Furthermore, the galvanostatic charge-discharge technique was reviewed using the CD-UR-Rad-Er 2018 instrument at a constant current density of 1.0 A g^{-1}. The specific capacitance, energy density, and power density are evaluated using the standard equation, stated as follows[38]

$$C_{sp} = \frac{I \cdot \Delta t}{m \cdot \Delta V}$$

$$E_{sp} = \frac{1}{2} C_{sp} \cdot \Delta V^2 \frac{1}{3.6}$$

$$P_{sp} = \frac{3600 \cdot E_{sp}}{t}$$

I is the current (A), Δt is the change in discharge time (s), m is the mass of activated carbon nanosheet, and ΔV is the change in discharge voltage (V). E_{sp} energy density (Wh kg^{-1}), and P_{sp} is power density (W kg^{-1}).

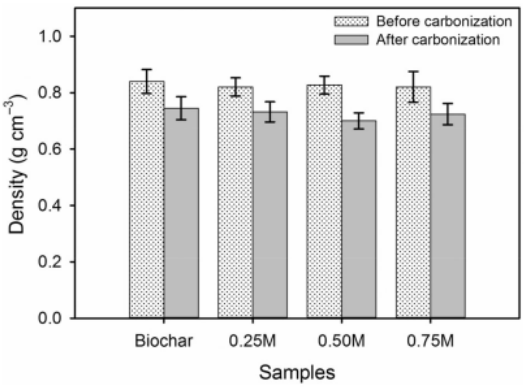

FIGURE 1 The change in density of solid pellet activated carbon

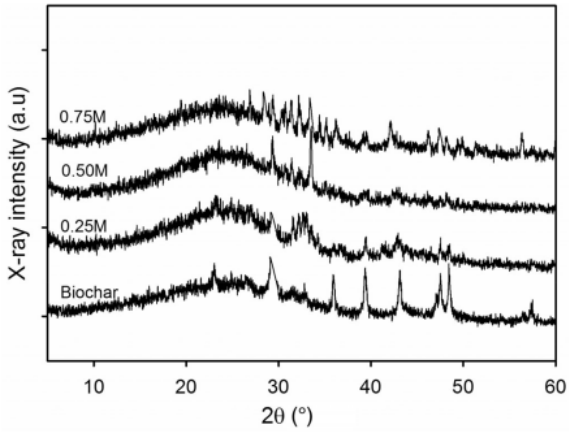

FIGURE 2 The XRD pattern of biochar, 0.25, 0.50, and 0.75 M

3 | RESULTS AND DISCUSSIONS

3.1 | Density confirmation

The impregnated zinc chloride and pyrolysis processes consisting of carbonization and physical activation in an N_2-CO_2 gas environment simultaneously affect the dimensions of pelleted activated carbon.[39] The mass, thickness, and diameter of the pellet were reduced regularly according to the heat treatment applied to the sample.[40] High-temperature pyrolysis decomposes basic biomass components such as hemicellulose, cellulose, and lignin.[41] Hemicellulose and cellulose decompose at relatively low temperatures ranging from 120°C to 240°C, and from 25°C to 380°C, respectively.[42] Lignin decomposes at a longer temperature ranging from 350°C to 900°C.[43] This process certainly reduces the dimensions of pelleted solids activated carbon. This is evident in the density change before and after the pyrolysis process, as shown in Figure 1. However, before the process, the density of all samples had approximately similar values of ±0.823 g cm^{-3} at average error of ±0.0425. After the carbonization and physical activation processes were completed, the carbon density decreased to 0.745, 0.732, 0.700, and 0.724 g cm^{-3} at average error of ±0.0282. The biochar sample showed a minimum density reduction of 9.47%. Conversely, the maximum density reduction of relatively 14.94% was determined in the 0.50 M sample. The zinc chloride concentration significantly affects the pelleted activated carbon activation, whereby the greater the given concentration, the greater the density reduction as confirmed in the biochar samples, 0.25 and 0.50 M. This is caused by the formation of excess ZnOCl from the reaction of carbon and $ZnCl_2$ at high temperatures.[44] Furthermore, the oxidative form of Zn tends to evaporate, thereby leaving a space in the sample. The increased evaporation of Zn in etching carbon chains creates a relatively large space in the sample, thereby reducing the density of the solid pellet. These empty spaces are often referred to as pores, and such behaviors are needed to improve the high performance of electrode material. Moreover, an increase in the $ZnCl_2$ concentration to 0.75 M indicates an increase in density due to the destruction of the pore wall structure. An excessive amount of $ZnCl_2$ reaction on carbon skeleton may drastically erode the pore walls, thus pore framework "collapses" and covers the pores below.[40,45] This density analysis is the initial reference in evaluating pelleted activated carbon's pore properties and surface area. It is further discussed using the N_2 gas adsorption or desorption analysis. As reported in previous studies, the density result obtained is considered normal for porous carbon derived from bio-waste.[45,46]

3.2 | Microstructure phase analysis

The activated carbon pellet nanosheets microstructure phase and particle arrangement were evaluated using the X-ray diffraction/XRD method. The XRD curves of the four-carbon nanosheet samples clearly showed broad peaks at 2θ = 24.412-25.437° angle, which correlates with the 002 planes, as shown in Figure 2. This confirms that the dominant amorphous carbon structure and the weak broad peak at the 2θ = 43.961-45.505° angle correlate with the 100 planes, partially forming a minor feature graphite-like structure.[47,48] In addition, the broad-peak at the 2θ (002) angle shifted to a smaller value from 25.437° to 24.412°, as shown in the biochar samples, 0.25, and 0.50 M. This is because the impregnated zinc chloride affects the turbostratic structure of the carbon.[49] The

Samples	$2\theta_{002}$ (°)	$2\theta_{100}$ (°)	d_{002} (Å)	d_{100} (Å)	L_c (Å)	L_a (Å)
Biochar	25.437	43.961	3.439	2.142	15.060	9.046
0.25 M	25.210	44.961	3.529	2.014	14.316	6.201
0.50 M	24.412	45.505	3.643	1.991	11.563	4.397
0.75 M	24.847	44.785	3.580	2.120	14.786	15.622

TABLE 1 The interlayer spacing the d_{002} and d_{100} and microcrystalline L_c and L_a dimensions

addition of zinc chloride concentration presents the formation of various pores in the sample, especially micropores and mesopores. However, at 0.75 M, 2θ (002) shifted back toward the larger at 24.647° indicating amorphous degradation. Furthermore, 2θ (100) shifted in a larger direction from 43.961° to 45.505° (from biochar samples to 0.50 M) indicating a rich nanopore structure.[48,49] This contrasts with 0.75 M confirming a decrease in their nanostructure. This property shifts the value of the angle 2θ (002) toward a larger one, as shown in Table 1. This feature causes porous carbon to have a high surface area as well as increases the supercapacitor device's energy. Furthermore, it is confirmed by pore size distribution analysis and GCD profile. In addition, the sample also shows few weak and sharp peaks, as confirmed on the XRD pattern. Biochar samples showed weak and sharp peaks at angles 29.7°, 37°, 40°, 43°, and 49°, indicating crystalline compounds such as SiO_2, MgO, $CaCO_3$, and SiO_2 due to incomplete evaporation of the biomass constituent elements (JCPDS: 89-1668, 89-7746, and 82-1690). Furthermore, zinc chloride impregnation succeeded in reducing the precursor sample's crystalline compound, thereby eliminating the sharp peak on the XRD curve. The EDS analysis further confirmed this, which showed highly pure carbon in zinc chloride impregnated samples.

Moreover, Table 1 comprehensively summarizes the interlayer spacing, the d_{002} and d_{100} planes as well as the microcrystalline L_c and L_a dimensions. The d_{002} value exhibits a relatively higher value of 10%-15% compared to that of the normal graphite d_{002}.[50] Therefore, this indicates that all samples have an irregular carbon structure, leading to amorphous substances. This is consistent with previous studies that reported activated carbon with an amorphous biomass structure such as mangosteen,[51] pitaya peel,[52] pineapple crown,[53] and orange peel.[54] Furthermore, the microcrystalline dimension L_c is associated with the prediction of the sample surface area, as stated in the previous empirical formula.[55] The L_c value is one of the parameters for evaluating surface area using the XRD technique. Additionally, the surface area is inversely proportional to the L_c value and graphite density. Based on this analysis, the increase in $ZnCl_2$ impregnation increases the sample surface area. The maximum surface area was discovered in 0.50 M $ZnCl_2$ impregnated samples. This speculation is further confirmed by analyzing N_2 gas adsorption or desorption.

3.3 | The morphological structure analysis

The morphological structure of pelletized activated carbon obtained from zinc chloride impregnated with different concentrations from 0.25 to 0.75 M was reviewed using SEM micrographs, as shown in Figure 3. Therefore, it is used to confirm the 2D nanosheet decorated with unique structures. In addition, zinc chloride impregnation exhibits various surface structures, including mesopores and macropores. Biochar as a precursor sample produces a unique morphology wooden labyrinth-like structure with a relatively smooth surface and relatively large pore block. High heat treatment etches the binding chain on lignin, cellulose, and hemicellulose components.[56] These components evaporate and degrade, thereby leading to unique structures.[57] Lignin and cellulose are the dominant contributors of tubular and microfiber structures in carbon-based biomass. This includes a unique structure resembling a wooden labyrinth. In the selected magnification area, biochar shows a nanosheet structure with a flat and smooth surface. Furthermore, zinc chloride and CO_2 reaction with carbon placed under high-temperature pyrolysis significantly changed the samples' morphology, as shown in Figure 3B. Zinc chloride impregnation drastically erodes the lignin and cellulose components and completely evaporates the hemicellulose.[58] This certainly changes the unique sample to a rod-like structure with a relatively rough surface, as shown in Figure 3B. Furthermore, 0.25 M has also been used to clearly demonstrate a 2D nanosheet structure followed by relatively meso-macropore-confirmed pore interconnections, as shown in the magnified area of Figure 3B. The obtained nanosheet structure has a relatively thin size within the range of ±26 nm. In addition, mesopores and macropores produce varying pore sizes ranging from 33 to 48 nm and 72 to 85 nm, respectively. The 2D nanosheet features decorated with various pores are needed to improve the electrode materials' performances as energy storage devices.[59] Moreover, increasing the concentration of zinc chloride in the 0.50 M sample

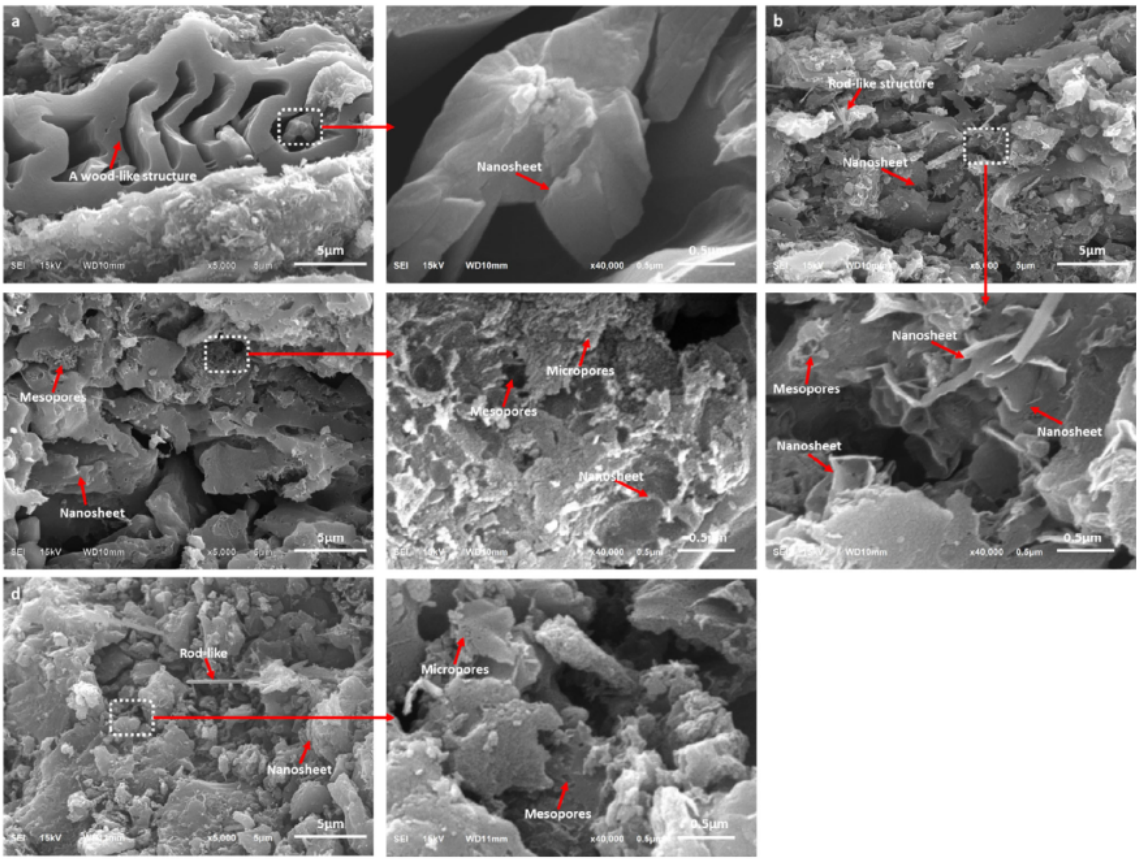

FIGURE 3 SEM image of (A) biochar, (B) 0.25 M, (C) 0.50 M, and (D) 0.75 M

optimizes the formation of pores on the surface, as shown in Figure 3C. Mesopores and macropores were found to be more diverse than 0.25 M samples with relative sizes ranging from 20 to 47 nm and 55 to 164 nm, respectively. The presence of a relatively large number of meso-macroporous pores significantly increases the ion diffusion rate on the electrode material surface, thereby causing electrolytes to move in all directions without any obstacles.[60,61] Furthermore, this treatment also affects the nanosheet structure thickness causing it to become thinner approximately ±15 nm. This leads to relatively short channels resulting in rapid ion transportation across the carbon matrix, thereby forming an electrical double layer. The combination of 2D nanosheet and meso-macroporous structure produces outstanding electrochemical properties of the supercapacitor electrode material,[32,33] as confirmed in the CV and GCD analysis. Moreover, increased zinc chloride concentration in the 0.75 M sample apparently eroded the 2D nanosheet structure determined by the SEM micrographs, as shown in Figure 3D. ZnO's by-product is in excess, causing the evaporated elemental zinc to erode the 2D nanosheet structure. Furthermore, this effect also erodes the carbon pore framework producing predominantly macropores with sizes ranging from 55 to 266 nm and mesopores of relatively 20 to 45 nm. Interestingly, the rod-like structure is persistent on the sample surface. As a comparison, several biomass sources showed similar potentials as *Moringa oleifera* stem[33] and *Syzygium oleana* leaves.[34]

3.4 | Elemental analysis

The elemental analysis of pelleted activated carbon was evaluated by employing the energy dispersive spectroscopy technique, shown in Table 2. The high-temperature pyrolysis treatment demonstrates the successful conversion of the bio-waste raw material to pure carbon content.[62] Biochar samples exhibited 76.79% of carbon, followed by oxygen as a contributor to oxidative compounds. Table 1 also shows the relatively high percentage of calcium compounds that correlates with the XRD

Samples	Elemental analysis						
	C (%)	O (%)	Mg (%)	Si (%)	Ca (%)	Cl (%)	K (%)
Biochar	76.79	20.12	0.30	0.53	2.26	0.00	0.00
0.25 M	85.32	11.32	0.35	0.36	2.48	0.11	0.07
0.50 M	88.68	9.78	0.17	0.27	0.92	0.15	0.02
0.75 M	90.32	7.57	0.22	0.43	1,20	0.26	0.00

TABLE 2 The elemental analysis of biochar, 0.25, 0.50, and 0.75 M

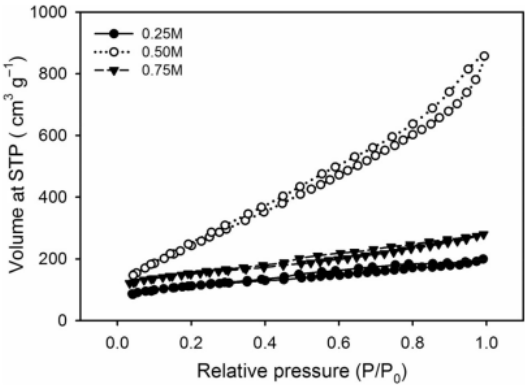

FIGURE 4 N_2 adsorption/desorption isotherms of activated carbon nanosheet

analysis. This indicates that the basic compounds constituting biomass calcium do not completely decompose only when heated. Furthermore, zinc chloride impregnated at different concentrations significantly increases carbon purity compared to biochar. Chemical impregnation, as well as the pyrolysis process, increases carbon purity by relatively 90.32%. In addition, contamination of the samples was drastically reduced, particularly oxygen and calcium. Furthermore, elemental chloride is found in minute percentages due to the chemical impregnation effect. The presence of magnesium and silicon elements in very small amounts are part of the constituent elements of biomass that are not degraded,[63] as found in the XRD pattern. Although the sample shows several contaminated compounds in relatively small amounts that increase the supercapacitor's resistance, the elemental oxygen exerts an attractive pseudo-capacitive effect on the electrode material, thereby boosting the device's performance.[64]

3.5 | Porosity features analysis

The pore characteristics of the garlic skin waste-based carbon nanosheets were further confirmed through the N_2 gas absorption/desorption. Figure 4 shows that the zinc chloride impregnated sample confirmed that types I and IV isotherms indicate a combination of interconnected micropore and mesoporous structures.[65] The absorption volume saturated at relatively low-pressure $P/P_0 < 0.35$ indicates mild micropore development. In addition, the hysteresis loop at a pressure of $0.40 < P/P_0 < 0.90$ causes mesopores to dominate the sample.[66] The increase in volume absorption at a relative pressure $P/P_0 > 0.96$ is associated with the macroporosity structure development.[67] Interestingly, the 0.50 M sample showed H3-type hysteresis loops, which were relatively different from 0.25 and 0.75 M, confirming the mesoporous structure is dominant due to the carbon matrix etching process. In addition, the 0.50 M sample showed the highest volume absorption confirming better pore characteristics compared to that of the 0.25 and 0.75 M. In detail, the porosity properties of chemically impregnated activated carbon are shown in Table 3. The 0.25 M impregnation showed a relatively low specific surface area at 366.320 $m^2\ g^{-1}$ with a total volume of 0.3089 $cm^3\ g^{-1}$. Interestingly, the sample showed a dominant mesoporous structure of 60.87% with a meso surface area (S_{meso}) of approximately 223.320 $m^2\ g^{-1}$. This is because, during the pyrolysis process, the reaction of zinc chloride with the carbon matrix occurs at an initial temperature of 500°C to produce ZnOCl by-products.[38,44] Further, this reaction continues till the maximum pyrolysis temperature of 850°C vaporizes the zinc oxide ZnO, and it etches the carbon chain matrix to form a dominant mesopore. This feature enhances the ionic charge transfer at the electrode or electrolyte interface. The addition of $ZnCl_2$ impregnation at a concentration of 0.50 M significantly increases the specific surface area by 273% of 1002.920 $m^2\ g^{-1}$ with a total volume of 1.3270 $cm^3\ g^{-1}$. This high surface area allows the electrolyte ions to form a large electrical double layer, thereby drastically increasing the energy density.[14,68] Furthermore, this speculation was confirmed by analyzing the electrochemical properties. In addition, the 0.50 M sample also showed an increase in mesoporosity by approximately 66.4% with a meso surface area (S_{meso}) of relatively 664.818 $m^2\ g^{-1}$. The high mesoporosity reduces the ESR resistance,

TABLE 3 The porosity features of biochar, 0.25, 0.50, and 0.75 M

Samples	S_{BET} ($m^2\ g^{-1}$)	S_{micro} ($m^2\ g^{-1}$)	S_{meso} ($m^2\ g^{-1}$)	V_{tot} ($cm^3\ g^{-1}$)	V_{micro} ($cm^3\ g^{-1}$)	V_{meso} ($cm^3 g^{-1}$)	D_{aver} (nm)
0.25 M	366.820	143.500	223.320	0.3089	0.1469	0.162	3.36
0.50 M	1002.920	338.102	664.818	1.3270	0.2190	1.108	5.29
0.75 M	486.209	167.700	318.509	0.4332	0.1992	0.234	3.56

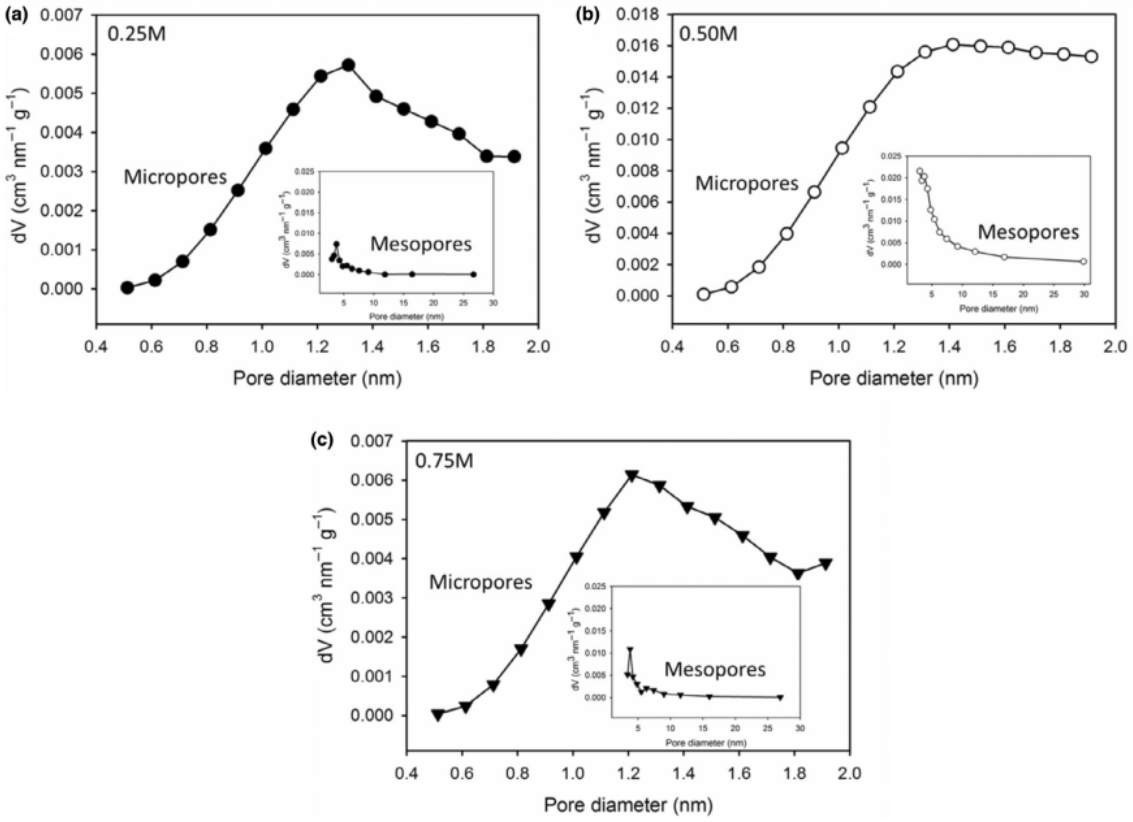

FIGURE 5 Pores size distribution of (A) 0.25 M, (B) 0.50 M, and (C) 0.75 M

thereby maintaining a high power density. This was further confirmed through resistance analysis using the galvanostatic charge-discharge method. Furthermore, the higher $ZnCl_2$ concentration in the 0.75 M sample decreased the high specific surface area of 486.209 $m^2\ g^{-1}$, with the total volume also degraded to 0.4332 $cm^3\ g^{-1}$. This is due to the pore framework erosion caused by excess zinc oxides, thereby making the carbon matrix unable to maintain its ideal structure, leading to its collapse and eradicating the possibility of expansion.[41,69] This also had an impact on the mesoporosity development, which fell to 65.5%. Figure 5A-C shows the pore size distribution for all zinc chloride impregnated samples. The three samples consistently showed a dominant mesopore (2 nm < x < 50 nm) size distribution with relatively variable volumes.[70] The 0.50 M sample produced the highest average pore size of 5.29 nm, while the 0.25 and 0.75 M samples were with 3.26 to 3.56 nm. These results are consistent with the SEM micrographs and dominant meso surface area. Interestingly, the samples also showed relatively evident sub-micropores (<0.7 nm) and ultra-micropores (0.8 nm < x < 2.0 nm).[71] These sub-ultra-micropores significantly improve capacitive performance due to the pore confinement effect as well as the provision of excess ion or electrode contact area.

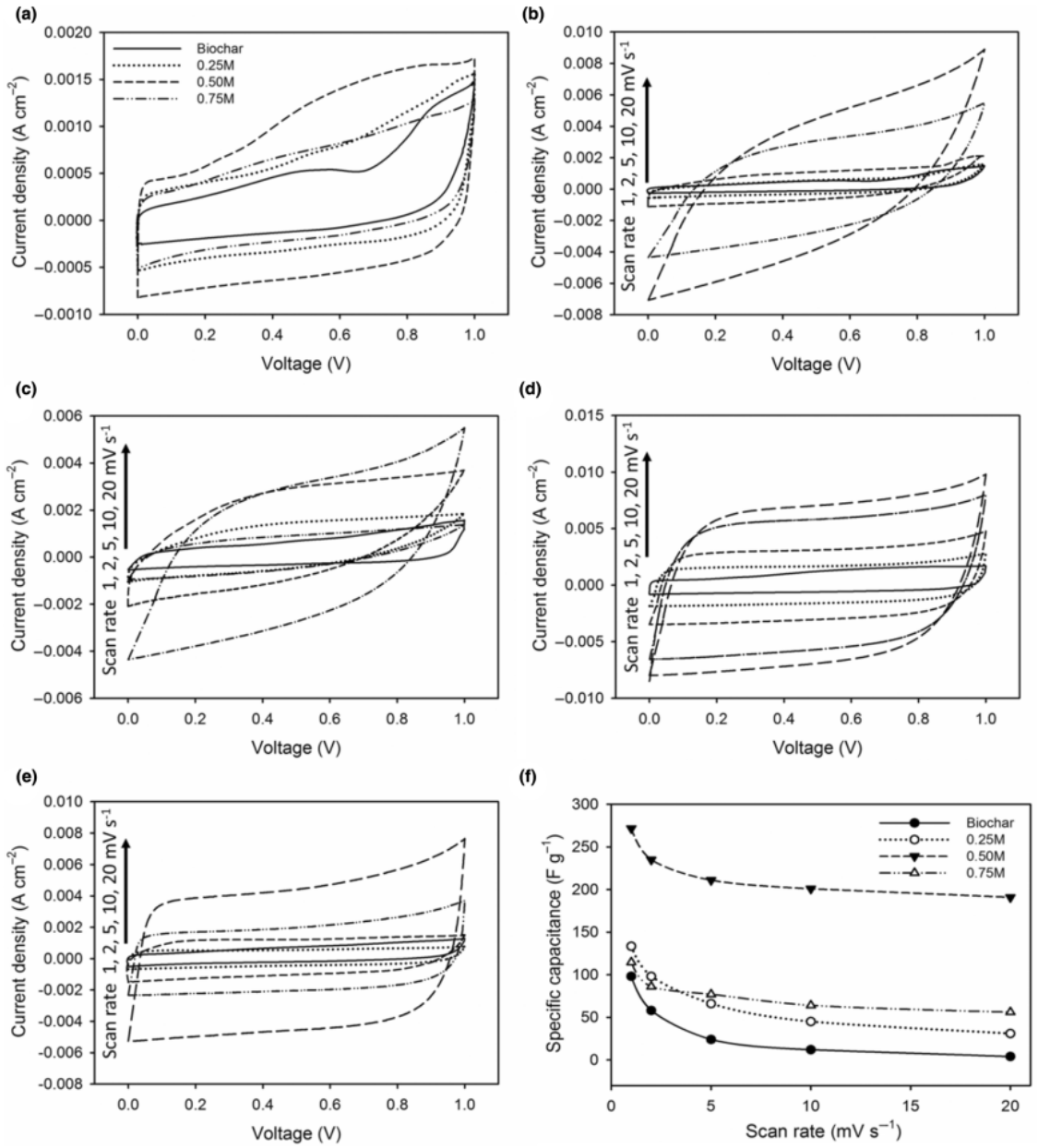

FIGURE 6 (A) CV profile of biochar, 0.25, 0.50, and 0.75 M at scan rate of 1 mV s^{-1}, CV profile in different scan rate of (B) biochar, (C) 0.25 M, (D) 0.50 M, (E) 0.75 M, and (F) specific capacitance in different scan rate of biochar, 0.25, 0.50, and 0.75 M

3.6 | Electrochemical behaviors analysis

The symmetric capacitive features of solid carbon pellets 2D nanosheet were evaluated using cyclic voltammetry and galvanostatic charge-discharge methods. Interestingly, the electrodes' electrochemical review was carried out without the use of adhesives such as PVA/PVDF/PTFE. The electrode was design in the form of disc/pellet carbon with two-electrode configuration system in 1 M H_2SO_4 electrolyte. Figure 6A shows a CV profile at a relatively low scan rate of 1 mV s^{-1} for all carbon nanosheet samples confirming the quasi-rectangular form. The double electrical layer capacitor behavior of the four sample variations was observed.[72] Furthermore, the inrush current density of 0.2 to 0.4 V indicates that the sample also has a pseudocapacitance effect due to the presence of

TABLE 4 The electrochemical behaviors of biochar, 0.25, 0.50, and 0.75 M

	CV			GCD			
Samples	C_{sp} (F g^{-1})	E_{sp} (Wh kg^{-1})	P_{sp} (W kg^{-1})	C_{sp} (F g^{-1})	E_{sp} (Wh kg^{-1})	E_{sp} (W kg^{-1})	R_s (mΩ)
Biochar	98.12	13.25	56.37	128.22	16.32	56.82	50
0.25 M	133.43	19.23	79.14	160.50	24.01	67.45	16
0.50 M	271.78	36.77	145.11	320.95	43.12	161.99	9
0.75 M	114.66	17.89	69.04	145.21	19.98	69.90	6

heteroatoms.[64,73] Oxygen as the second-highest element is considered a self-doping heteroatom that causes a faradic redox reaction in the electrode material.[74,75] This also affects the supercapacitors' performance. Several similar cases were also discovered using raw materials from banana leaves,[25] orange peel,[76] and jackfruit peel.[77] Based on Equation 1, the specific capacitance obtained from the carbon nanosheet electrodes is 123.55, 155.86, 286.34, 130.34 F g^{-1} for biochar sample, 0.25, 0.50, and 0.75 M, respectively. The 2D nanosheet structure on the biochar sample, which was not chemically activated, has resulted in relatively high capacitive properties. The application of 0.25 M zinc chloride impregnation showed an increase in capacitive properties, increasing by 26.15%. This was based on previously confirmed studies carried out on nanosheet structure and mesoporosity, as shown in Figure 3B. Furthermore, increasing the $ZnCl_2$ concentration to 0.50 M surprisingly increased the specific capacitance to approximately 131.76%. Additionally, the electrodes' specific energy and power also showed a drastic increase, as shown in Table 4. The high specific surface area with an increase of approximately 264% allows the provision of abundant ionic charge contact areas. This causes excess ionic charges to diffuse at the electrode or electrolyte interface, thereby generating a high electric double layer. In addition, the relatively thin nanosheet structure of 15 nm permits the use of short ion channels; therefore, its transportation is faster throughout the carbon matrix. These features significantly improve the electrode material performance to obtain excellent electrochemical properties.[32,78] However, the microstructural degradation, low specific surface area, and loss of 2D nanosheet structure in the 0.75 M sample reduced the capacitive property compared to previous samples. Figure 6B-E shows the carbon nanosheet CV profile at different scanning rates of 1, 2, 5, 10, and 20 mV s^{-1}. All samples consistently displayed a quasi-rectangular profile confirming the normal electrical layers properties. Biochar samples maintained high current spikes within the range of 0.8 to 1.0 V, indicating the presence of macroporosity at sizes of approximately 100 to 500 nm. Furthermore, $ZnCl_2$ impregnated at 0.25, 0.50, and 0.75 M samples showed a reduction in the faradaic redox reaction as the scanning rate increased. This is due to the oxygen content is unable to act as a self-doping at relatively high currents. An increase in the scanning rate from 1 to 20 mV s^{-1} evaluates the electrode material performance, as shown in Figure 6F. The specific capacitance decreases with an increase in the scanning rate, indicating that the ionic charge is unable to fill all pores framework due to the relatively narrow transport paths. However, the 0.50 M sample maintains A high-rate capability of approximately 68.53% with specific capacitance of 198 F g^{-1} because it has the highest mesoporosity; therefore, it smoothly opens the ion transport pathway in forming an electrical double-layer.[6,79]

Furthermore, the electrochemical properties were further evaluated through a galvanostatic charge-discharge technique with a symmetric supercapacitor system at a constant current density of 1.0 A g^{-1} in 1 M H_2SO_4 aqueous electrolyte. As shown in Figure 7A, the GCD profiles for biochar, 0.25, 0.50, and 0.75 M show a distorted triangular shape indicating normal electrical double layer properties. This corresponds to the CV profile shown in Figure 6A. The distorted triangle type shows eximious charge or discharges reversibility at different times for all samples. The 0.50 M sample has the longest charge-discharges time confirming that it has excellent electrochemical properties. In detail, the 0.50 M sample exhibits a specific capacitance, energy, and power of 320.95 F g^{-1}, 44.52 Wh kg^{-1}, and 155.20 W kg^{-1}, at a constant current density of 1.0 A g^{-1}, respectively. This value is higher than other samples such as biochar samples, 0.25 M and 0.75 M, which shows specific capacitances of 128.22, 160.50, and 145.21 F g^{-1}, as shown in Table 4. The trend is suitable and confirms data and CV analysis that was previously obtained. The high electrochemical performance in the 0.50 M sample was obtained from the relatively thin 2D nanosheet of 15 nm structure and decorated by the interconnected micro-mesoporosity structure which facilitates the formation of an electric layer and ion charge transport pathway at the electrode/electrolyte interface, thereby leading to high capacity rate capability.[59,80] In addition, the high oxygen content acts

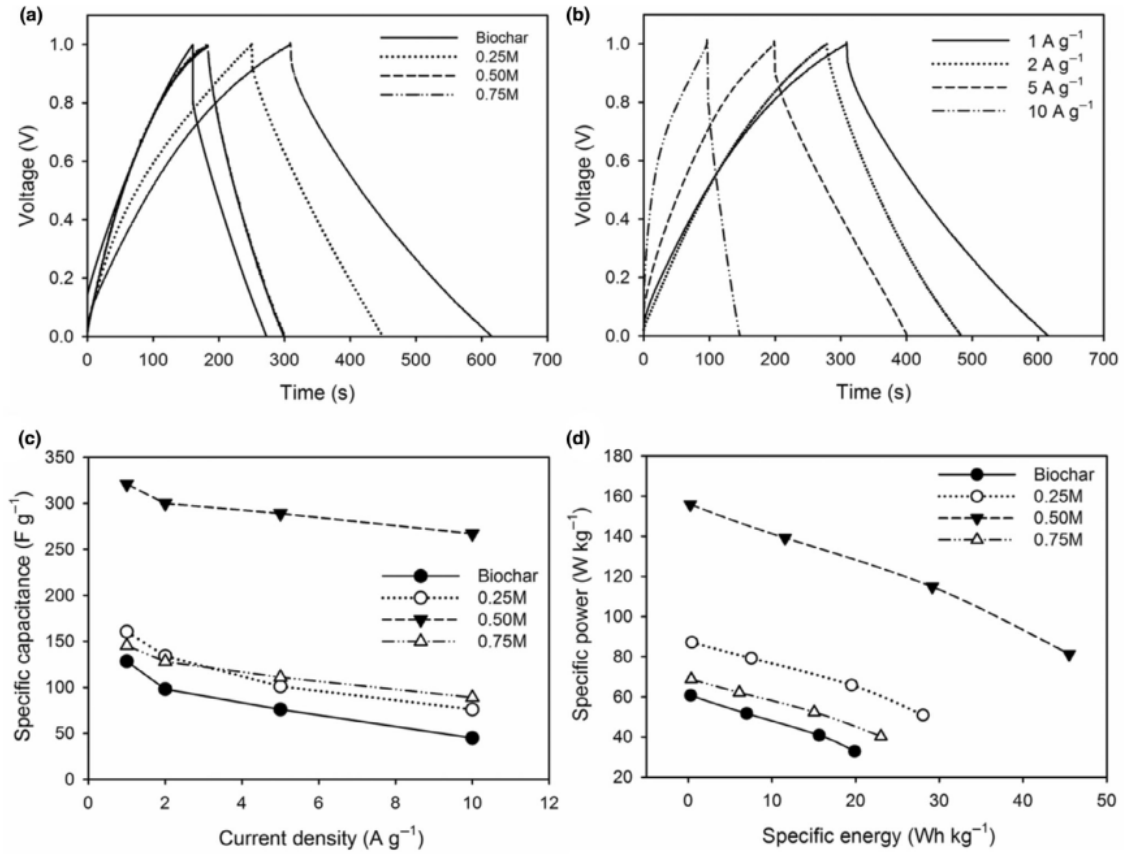

FIGURE 7 (A) GCD profile at 1.0 A g^{-1}, (B) The specific capacitance vs different current density, and (C) Ragone plot of biochar, 0.25, 0.50, and 0.75 M

as a self-doping which is useful for increasing the electronic conductivity and surface wettability of the carbon material, thereby improving the electrode material performance.[81,82] In addition, iR drop was also observed in the GCD profile. Biochar samples indicated the highest resistance reached 50mΩ due to the presence of contamination in the sample. Furthermore, zinc chloride impregnation of 0.25, 0.50, and 0.75 M samples showed a decrease in resistance of 16, 9, and 6 mΩ, respectively. This is because an increase in chemical impregnation significantly increased the mesoporosity structural development by relatively 66.83%,[6] as confirmed by the morphological analysis and N_2 adsorption or desorption. In addition, 0.50 M electrode was reviewed at higher current density of 1-10 A g^{-1}, as shown in Figure 7B. The GCD curve of 0.50 M still maintains symmetric triangle shape at 10 A g^{-1} suggesting normal double-layer capacitor behaviors, fast ion response, and low internal resistance in EDL processes.[42] As Shown in Figure 7C, different current density can reduce specific capacitance of all samples. However, 0.50 M sample possessed a high-rate performance of 78.9% at 10 A g^{-1}.

Furthermore, the symmetric supercapacitor-specific energy and power were thoroughly evaluated for the four different samples, as shown in Figure 7D. The Ragone plot shows the specific energy and specific power in Biochar, 0.25, 0.50, and 0.75 M samples at a current density of 1-10 Ag^{-1}. It needs to be noted, that the 0.50 M sample showed the highest relative specific energy of 43.12 Wh kg^{-1} with a maximum increase of 125.41% at a power density of 161.99 W kg^{-1} compared to the biochar sample, which was only approximately 16.32 Wh kg^{-1}. This result is consistent with the CV analysis. This is ascribed to a confirmed super-microporous structure followed by a high mesoporosity in 0.50 M. In addition, oxygen self-doping contributes to the improvement of their electrochemical properties.

To further corroborate the high CV and GCD electrochemical performance of the 0.50 M electrode, we performed alternating current-based electrochemical

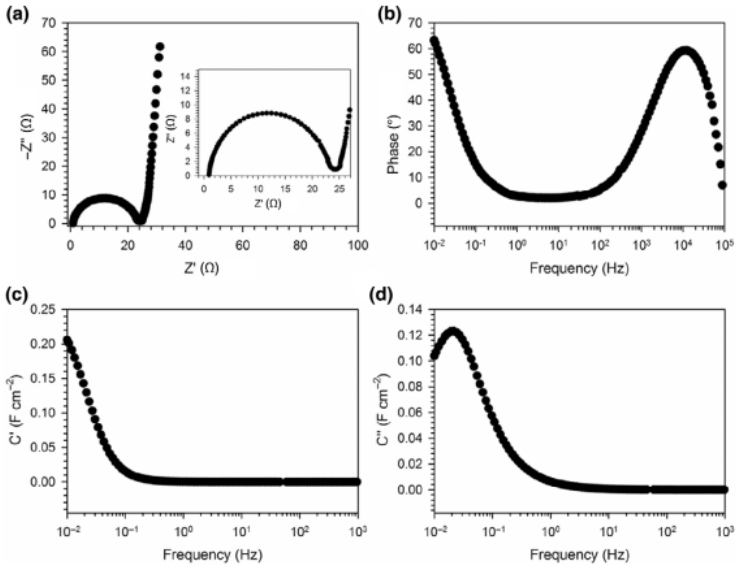

FIGURE 8 (A) Nyquist plot, (B) bode plot, (C) real capacitance (C′) vs frequency plot, and (D) imaginer capacitance (C′′) vs frequency plot of 0.50 M symmetrical devices

impedance spectroscopy as shown in Figure 8. The Nyquist plots and the bode plots obtained provide detailed information on the accessibility and migration of electrolyte ions, which depend on the pore size of the electrode.[47] This behavior is reviewed at low to high frequencies in the range of 0.01-100 000 Hz at the amplitude of 10 mV. Figure 8A discloses a Nyquist plot confirming a low charge transfer resistance of about 0.98 Ωcm^{-2} with an electrolyte ionic resistance of 0.15 Ωcm^{-2}. In addition, Warburg's vertical lines at higher frequencies exhibit characteristic capacitive behavior and high cell conductivity.[47,48] Figure 8B shows the frequency-dependent phase angle, where the low-frequency phase angle close to −90 indicates an electric double layer type that has extra pseudo-capacitance.[52] Furthermore, the confirmed peak at high frequency is associated with the diffusion resistance of the supercapacitor cell circuit. Furthermore, the bode plot represented by the real capacitance (C′) as a function of frequency evaluates the amount of electrolytic charge reaching the porous carbon interface over a certain frequency range.[53] At low frequencies, the entire 0.50 M electrode surface is accessible to the electrolyte ion which results in a markedly high capacitance relation. The larger increase in frequency tends to decrease the apparent capacitance which further proves the importance of the small ion pathways required to achieve higher performance.[62] Moreover, Figure 8D presents a plot of the imaginary capacitance (C′′) as a function of frequency, which represents the relaxation time constant. This parameter confirms the minimum time required to discharge the energy device voltage with efficiency. The relaxation time constant was evaluated using the equation $\tau = 1/2\pi f_p$, where f_p is the peak frequency of each 0.50 M electrode. The 0.05 M electrode exhibits a short relaxation time of approximately 34.51 ms. This results indicate that the 0.05 M symmetrical electrode has an ultra-fast and excellent ion adsorption/desorption rate capability. In comparison, the maximum energy density at 0.50 M is higher than the recently reported porous carbon symmetrical cells such as bacterial cellulose carbon-based[83] and conducting polymer nanosheet-based supercapacitors[21] as shown in Table 5. These analyses have proven the successful conversion of bio-waste into highly micro-mesopores activated carbon solid pellet 2D nanosheet, electrode materials for energy storage.

4 | CONCLUSIONS

In summary, free-template and free-binder synthesis of highly porous carbon nanosheet was successfully demonstrated from garlic skin precursor through zinc chloride impregnation at high-temperature pyrolysis in N_2/CO_2 gas atmosphere. Garlic skin wastes were converted into activated carbon in the form of solid pellets, excluding synthetic adhesive compounds. The raw material components' unique structure is maintained by applying chemical impregnations at relatively low concentrations of 0.25, 0.50, and 0.75 M. Combining the unique structure and 2D nanosheets in the 0.50 M sample surprisingly boosts the specific surface area by approximately 273% and is dominated by a high mesoporosity structure of relatively 66.4%. In addition, the relatively high oxygen

TABLE 5 The comparison of electrochemical behavior supercapacitor in different sources

Carbon sources	Method	Morphological	S_{BET} ($m^2\ g^{-1}$)	Binder	Electrolyte	Current density ($A\ g^{-1}$)	C_{sp} ($F\ g^{-1}$)	E_{sp} ($Wh\ kg^{-1}$)	P_{sp} ($W\ kg^{-1}$)	Refs
Bacterial cellulose	silica-assisted	Micro-mesopores nanofiber	624	Free-binder	6 M KOH	0.5	302	6.9	128.4	84
EDTA-Na_2Zn	Template-assisted	Holey nanosheet	701.7	-	2 M KOH	2.0	205	17.92	500	21
Native European deciduous trees	Cavitation process	interconnected pores	614	PVDF	1 M H_2SO_4	0.25	24	0.53	51	63
Chitin nanofiber	Bio-templates	hierarchically porous	876	PTFE	6 M KOH	0.2	128.5	4.46	50	85
Moringa oleifera	One-step pyrolysis	Hierarchically porous nanosheet	2250	PTFE	1 M Na_2SO_4	0.5	283	25.8	89	33
L-cysteine	NaCl template	Nanosheet	1552	PTFE	6 M KOH	0.5	363.1	13.4	325	78
Syzygium oleana leaves	One-stage integrated pyrolysis	Nanosheet	1218	Free-binder	1 M H_2SO_4	-	188	26	96	34
Garlic skin	$ZnCl_2$ impregnation	Nanosheet	1002.92	Free-binder	1 M H_2SO_4	1.0	320.95	44.52	155.87	This work

content elicits a redox faradaic reaction effect, thereby confirming the high wettability properties and increased electrical conductivity of the electrode material. This superior property improves the supercapacitor symmetric electrochemical performance to relatively 131.45% with a specific capacitance of 320.95 F g^{-1} at a constant current density of 1.0 A g^{-1}. Furthermore, specific energy and power were also evaluated in 1M H_2SO_4 electrolyte 43.12 and 161.99 Wh kg^{-1}, respectively. However, compared to previously established techniques, the preparation of activated carbon 2D nanosheets with micro-mesoporous interconnections understudy is easier, efficient, controllable, and environmentally friendly, thereby generating high potential for energy storage applications.

ACKNOWLEDGEMENTS

The research was supported by second year Project of Word Class Research (WCR) in *Kementerian pendidikan, Kebudayaan, Riset, dan Teknologi*, Republic of Indonesia with contract No: 1627/UN19.5.1.3/PT.01.03/2022. Project title: "*Superkapasitor dengan Rapat Energi dan Daya Tinggi: Optimalisasi Proses Penyediaan Elektroda*."

ORCID

Erman Taer https://orcid.org/0000-0003-4463-8252

REFERENCES

1. Kalyani P, Anitha A. Biomass carbon & its prospects in electrochemical energy systems. *Int J Hydrogen Energy*. 2013;38:4034-4045.
2. Simon P, Burke A. Nanostructured carbons: double-layer capacitance and more. *Electrochem Soc Interface*. 2008;17:38-43.
3. González A, Goikolea E, Barrena JA, Mysyk R. Review on supercapacitors: technologies and materials. *Renew Sustain Energy Rev*. 2016;58:1189-1206.
4. Du D, Wang Li S, et al. Remarkable supercapacitor performance of petal-like LDHs vertically grown on graphene/polypyrrole nanoflakes. *J Mater Chem A*. 2017;5:8964-8971.
5. Poonam P, Sharma K, Arora A, Tripathi SK. Review of supercapacitors: materials and devices. *J Energy Storage*. 2019;21:801-825.
6. Liu D, Zhang W, Huang W. Effect of removing silica in rice husk for the preparation of activated carbon for supercapacitor applications. *Chin Chem Lett*. 2019;30:1315-1319.
7. Ding C, Liu T, Yan X, et al. An ultra-microporous carbon material boosting integrated capacitance for cellulose-based supercapacitors. *Nano-Micro Lett*. 2020;12:63.
8. Liu X, Ma C, Li J, et al. Biomass-derived robust three-dimensional porous carbon for high volumetric performance supercapacitors. *J Power Sources*. 2019;412:1-9.
9. Macías-García A, Torrejón-Martín D, Díaz-Díez MÁ, Carrasco-Amador JP. Study of the influence of particle size of activate carbon for the manufacture of electrodes for supercapacitors. *J Energy Storage*. 2019;25:100829.
10. Kumar R, Sahoo S, Joanni E, et al. Recent progress in the synthesis of graphene and derived materials for next generation electrodes of high performance lithium ion batteries. *Prog Energy Combust Sci*. 2019;75:100786.
11. Young C, Park T, Yi JW, et al. Advanced functional carbons and their hybrid nanoarchitectures towards supercapacitor applications. *ChemSusChem*. 2018;11:3546-3558.
12. Lu Z, Foroughi J, Wang C, Long H, Wallace GG. Superelastic hybrid CNT/graphene fibers for wearable energy storage. *Adv Energy Mater*. 2018;8:1-10.
13. Palisoc S, Dungo JM, Natividad M. Low-cost supercapacitor based on multi-walled carbon nanotubes and activated carbon derived from *Moringa oleifera* fruit shells. *Heliyon*. 2020;6:e03202.
14. Wu J, Xia M, Zhang X, et al. Hierarchical porous carbon derived from wood tar using crab as the template: performance on supercapacitor. *J Power Sources*. 2020;455:227982.
15. Dobele G, Dizhbite T, Gil MV, Volperts A, Centeno TA. Production of nanoporous carbons from wood processing wastes and their use in supercapacitors and CO_2 capture. *Biomass Bioenergy*. 2012;46:145-154.
16. Qi J, Mao J, Zhang A, et al. Facile synthesis of mesoporous $ZnCo_2O_4$ nanosheet arrays grown on rGO as binder-free electrode for high-performance asymmetric supercapacitor. *J Mater Sci*. 2018;53:16074-16085.
17. Zang S, Jiang J, An Y, et al. A novel porous organic polymer-derived hierarchical carbon for supercapacitors with ultrahigh energy density and durability. *J Electroanal Chem*. 2020;876:114723.
18. Wang S, Tan C, Fei L, et al. Rational design and in-situ synthesis of ultra-thin β-$Ni(OH)_2$ Nanoplates for high performance all-solid-state flexible supercapacitors. *Front Chem*. 2020;8:1-9.
19. Gopalakrishnan A, Raju TD, Badhulika S. Green synthesis of nitrogen, sulfur-co-doped worm-like hierarchical porous carbon derived from ginger for outstanding supercapacitor performance. *Carbon N Y*. 2020;168:209-219.
20. Fu H, Zhang X, Fu J, et al. Single layers of MoS_2/Graphene nanosheets embedded in activated carbon nanofibers for high-performance supercapacitor. *J Alloys Compd*. 2020;829:154557.
21. Peng H, Qi S, Miao Q, et al. Formation of nitrogen-doped holey carbon nanosheets via self-generated template assisted carbonization of polyimide nanoflowers for supercapacitor. *J Power Sources*. 2021;482:228993.
22. Xie A, Dai J, Chen Y, et al. NaCl-template assisted preparation of porous carbon nanosheets started from lignin for efficient removal of tetracycline. *Adv Powder Technol*. 2019;30:170-179.
23. Guo S, Chen Y, Shi L, et al. Nitrogen-doped biomass-based ultra-thin carbon nanosheets with interconnected framework for High-Performance Lithium-Ion Batteries. *Appl Surf Sci*. 2018;437:136-143.
24. Huo S, Liu M, Wu L, et al. Synthesis of ultrathin and hierarchically porous carbon nanosheets based on interlayer-confined inorganic/organic coordination for high performance supercapacitors. *J Power Sources*. 2019;414:392.
25. Roy CK, Shah SS, Reaz AH, et al. Preparation of hierarchical porous activated carbon from banana leaves for high-performance supercapacitor: effect of type of electrolytes on performance. *Chemistry – Asian J*. 2021;16:296-308.

26. Taer E, Taslim R. Brief review: preparation techniques of biomass based activated carbon monolith electrode for supercapacitor applications. *AIP Conf Proc*. 1927;2018:020004.
27. Mishra RK, Ha SK, Verma K, Tiwari SK. Recent progress in selected bio-nanomaterials and their engineering applications: an overview. *J Sci Adv Mater Devices*. 2018;3:263-288.
28. Yang CS, Jang YS, Jeong HK. Bamboo-based activated carbon for supercapacitor applications. *Curr Appl Phys*. 2014;14:1616-1620.
29. Kumar TR, Senthil RA, Pan Z, Pan J, Sun Y. A tubular-like porous carbon derived from waste American poplar fruit as advanced electrode material for high-performance supercapacitor. *J Energy Storage*. 2020;32:1[illegible]3.
30. Ma X, Wang H, Wu Q, et al. Bamboolike carbon microfibers derived from typha orientalis fibers for supercapacitors and capacitive deionization. *J Electrochem Soc*. 2019;166:A236-A244.
31. Wu X, Hong X, Luo Z, et al. The effects of surface modification on the supercapacitive behaviors of novel mesoporous carbon derived from rod-like hydroxyapatite template. *Electrochim Acta*. 2013;89:400-406.
32. Selvaraj AR, Muthusamy A, ho-Cho I, Kim HJ, Senthil K, Prabakar K. Ultrahigh surface area biomass derived 3D hierarchical porous carbon nanosheet electrodes for high energy den- supercapacitors. *Carbon N Y*. 2020;174:463-474.
33. Cai Y, Luo Y, Dong H, et al. Hierarchically porous carbon nanosheets derived from *Moringa oleifera* stems as electrode material for high-performance electric double-layer capacitors. *J Power Sources*. 2017;353:260-269.
34. Taer E, Apriwandi A, Taslim R, Agutino A, Yusra DA. Conversion *Syzygium oleana* leaves biomass waste to porous activated carbon nanosheet for boosting supercapacitor performances. *Mater Res Technol*. 2020;9:13332-13340.
35. Sodtipinta J, Ieosakulrat C, Poonyayant N, et al. Interconnected open-channel carbon nanosheets derived from pineapple leaf fiber as a sustainable active material for supercapacitors. *Ind Crops Prod*. 2017;104:13-20.
36. Yaya A, Agyei-Tuffour B, Dodoo-Arhin D, et al. Layered nanomaterials–a review. *Glob J Eng Des Technol*. 2012;1:32-41.
37. Taer E, Yanti [illegible], Mustika WS, Apriwandi A, Taslim R, Agustino A. Porous activated carbon monolith with nanosheet/nanofiber structure derived from the green stem of cassava for supercapacitor application. *Int J Energy Res*. 2020;44:1-14.
38. Hor AA, Hashmi SA. Optimization of hierarchical porous carbon derived from a biomass pollen-cone as high-performance electrodes for supercapacitors. *Electrochim Acta*. 2020;356:136826.
39. Farma R, Deraman M, Omar R, et al. Binderless composite electrode monolith from carbon nanotube and biomass carbon activated by KOH and CO_2 gas for supercapacitor. *AIP Conf Proc*. 2011;1415:180-184.
40. Apriwandi A, Taer E, Farma R, Setiadi RN, Amiruddin E. A facile approach of micro-mesopores structure binder-free coin/monolith solid design activated carbon for electrode [illegible]ercapacitor. *J Energy Storage*. 2021;40:102823.
41. Erabee IK, Ahsan A, Zularisam AW, et al. A new activated carbon prepared from sago palm bark through physiochemical activated process with zinc chloride. *Eng J*. 2017;21:1-14.
42. Kim J, Won H, Min S, Jae J, Park Y. Overview of the recent advances in lignocellulose liquefaction for producing biofuels, bio-based materials and chemicals. *Bioresour Technol*. 2019;[illegible]373-384.
43. Samanta AK, Basu G, Mishra L. Role of major constituents of coconut fibres on absorption of ionic dyes. *Ind Crops Prod*. [illegible]8;117:20-27.
44. Boyjoo Y, Cheng Y, Zhong H, et al. From waste Coca Cola® to activated carbons with impressive capabilities for CO_2 adsorption and supercapacitors. *Carbon N Y*. 2017;116:490-499.
45. Taer E, Natalia K, Apriwandi A, Taslim R, Agustino A, Farma R. The synthesis of activated carbon nano fiber electrode made from acacia leaves (*Acacia mangium wild*) as supercapacitors. *Adv Nat Sci Nanosci Nanotechnol*. 2020;11:025007.
46. Taer E, A[illegible]anda A, Apriwandi A, Taslim R, Agustino A, Farma R. Production of activated carbon electrodes from sago waste and its application for an electrochemical double-layer [illegible]acitor. *Int J Electrochem Sci*. 2018;13:10688-10699.
47. Martínez-Casillas [illegible]DC, Mascorro-Gutiérrez I, Arreola-Ramos CE, et al. A sustainable approach to produce activated carbons from pecan nutshell waste for environmentally [illegible]ndly supercapacitors. *Carbon N Y*. 2019;148:403-412.
48. Márquez-Montesino F, Torres-Figueredo N, Lemus-Santana A, Trejo F. Activated carbon by potassium carbonate activation from pine sawdust (*Pinus montezumae* Lamb.). *Chem Eng [illegible]nol*. 2020;43:1716-1725.
49. Girgis BS, Temerk YM, Gadelrab MM, Abdullah ID. X-ray diffraction patterns of activated carbons prepared under various [illegible]ditions. *Carbon Sci*. 2007;8:9[illegible]00.
50. Serafin J, Baca M, Biegun M, et al. Direct conversion of biomass to nanoporous activated biocarbons for high CO_2 adsorption and supercapacitor applications. *Appl Surf Sci*. 2019;497:143722.
51. Yang V, Senthil RA, Pan J, et al. Highly ordered hierarchical porous carbon derived from biomass waste mangosteen peel as superior cathode material for high performance supercapacitor. *[illegible]ectroanal Chem*. 2019;19:113616.
52. Lu W, Cao X, Hao L, Zhou Y, Wang Y. Activated carbon derived from pitaya peel for supercapacitor applications with high capacitance performance. *Mater Lett*. 2020;264:127339.
53. Taer E, Apriwandi A, Dalimunthe BKL, Taslim R. A rod-like mesoporous carbon derived from agro-industrial cassava petiole waste for Supercapacitor application. *J Chem Technol Biotechnol*. 2021;96:662-671.
54. Gou H, He J, Zhao G, Zhang L, Yang C, Rao H. Porous nitrogen-doped carbon networks derived from orange peel for high-performance supercapacitors. *Ionics (Kiel)*. 2019;25:4371-4380.
55. Deraman M, Daik R, Soltaninejad S, et al. A new empirical equation for estimating specific surface area of supercapacitor carbon electrode from X-ray diffraction. *Adv Mater Res*. 2015;1108:1-7.
56. de Luna MY, Rodrigues PM, Torres GAM, et al. A thermogravimetric analysis of biomass wastes from the northeast region of Brazil as fuels for energy recovery. *Energy Sour Part A: Recov Util Environ Eff*. 2018;41:1557-1575.
57. Jiang W, Pan J, Liu X. A novel rod-like porous carbon with ordered hierarchical pore structure prepared from Al-based metal-organic framework without template as greatly

enhanced performance for supercapacitor. *J Power Sources*. 2019;409:13-23.
58. Sun Q, Jiang T, Zhao G, Shi J. Porous carbon material based on biomass prepared by MgO template method and $ZnCl_2$ activation method as electrode for high performance supercapacitor. *Int J Electrochem Sci*. 2019;14:1-14.
59. Yang X, Kong L, Cao M, Liu X, Li X. Porous nanosheets-based carbon aerogel derived from sustainable rattan for supercapacitors application. *Ind Crops Prod*. 2020;145:112100.
60. Wan L, Song P, Liu J, et al. Facile synthesis of nitrogen self-doped hierarchical porous carbon derived from pine pollen via $MgCO_3$ activation for high-performance supercapacitors. *J Power Sources*. 2019;438:227013.
61. Wang Y, Qiao M, Mamat X. Nitrogen-doped macro-meso-micro hierarchical ordered porous carbon derived from ZIF-8 for boosting supercapacitor performance. *Appl Surf Sci*. 2021;540:148352.
62. Wang G, Zhang L, Zhang J. A review of electrode materials for electrochemical supercapacitors. *Chem Soc Rev*. 2012;41:797-828.
63. Jain A, Ghosh M, Krajewski M, Kurungot S, Michalska M. Biomass-derived activated carbon material from native European deciduous trees as an inexpensive and sustainable energy material for supercapacitor application. *J Energy Storage*. 2021;34:102178.
64. Ghosh S, Barg S, Jeong SM, Ostrikov K. Heteroatom-doped and oxygen-functionalized nanocarbons for high-performance supercapacitors. *Adv Energy Mater*. 2020;10:1-44.
65. Sing KSW. Reporting physisorption data for gas/solid systems with special reference to the determination of surface area and porosity. *Pure Appl Chem*. 1982;54:2201-2218.
66. Zhang WL, Xu JH, Hou DX, et al. Hierarchical porous carbon prepared from biomass through a facile method for supercapacitor applications. *J Colloid Interface Sci*. 2018;530:338-344.
67. Zhang Y, Yu S, Lou G, et al. Review of macroporous materials as electrochemical supercapacitor electrodes. *J Mater Sci*. 2017;52:11201-11228.
68. Sun K, Zhang Z, Peng H, Zhao G, Ma G, Lei Z. Hybrid symmetric supercapacitor assembled by renewable corn silks based porous carbon and redox-active electrolytes. *Mater Chem Phys*. 2018;218:229-238.
69. Saka C. BET, TG-DTG, FT-IR, SEM, iodine number analysis and preparation of activated carbon from acorn shell by chemical activation with $ZnCl_2$. *J Anal Appl Pyrolysis*. 2012;95:21-24.
70. Wei X, Wei JS, Li Y, Zou H. Robust hierarchically interconnected porous carbons derived from discarded Rhus typhina fruits for ultrahigh capacitive performance supercapacitors. *J Power Sources*. 2019;414:13-23.
71. Chiang YC, Lee ST, Leo YJ, Tseng TL. Importance of pore structure and surface chemistry in carbon dioxide adsorption on electrospun carbon nanofibers. *Sens Mater*. 2020;32:2277-2288.
72. Pina A, Amaya A, Marcuzzo J, et al. Supercapacitor electrode based on activated carbon wool felt. *J Carbon Res*. 2018;4:24.
73. Abbas Q, Raza R, Shabbir I, Olabi AG. Heteroatom doped high porosity carbon nanomaterials as electrodes for energy storage in electrochemical capacitors: a review. *J Sci Adv Mater Devices*. 2019;4:341-352.
74. Wang K, Zhao N, Lei S, et al. Promising biomass-based activated carbons derived from willow catkins for high performance supercapacitors. *Electrochim Acta*. 2015;166:1-11.
75. Yang H, Zhou J, Wang M, Wu S, Yang W, Wang H. From basil seed to flexible supercapacitors: green synthesis of heteroatom-enriched porous carbon by self-gelation strategy. *Int J Energy Res*. 2020;44:4449-4463.
76. Wan L, Chen D, Liu J, et al. Facile preparation of porous carbons derived from orange peel via basic copper carbonate activation for supercapacitors. *J Alloys Compd*. 2020;823:153747.
77. Foo KY, Hameed BH. Potential of jackfruit peel as precursor for activated carbon prepared by microwave induced NaOH activation. *Bioresour Technol*. 2012;112:143-150.
78. Guo Y, Wang T, Wu D, Tan Y. One-step synthesis of in-situ N, S self-doped carbon nanosheets with hierarchical porous structure for high performance supercapacitor and oxygen reduction reaction electrocatalyst. *Electrochim Acta*. 2021;366:137404.
79. Tian X, Zhu S, Peng J, et al. Synthesis of micro- and mesoporous carbon derived from cellulose as an electrode material for supercapacitors. *Electrochim Acta*. 2017;241:170-178.
80. Zhang G, Guan T, Cheng M, et al. Harvesting honeycomb-like carbon nanosheets with tunable mesopores from mild-modified coal tar pitch for high-performance flexible all-solid-state supercapacitors. *J Power Sources*. 2020;448:227446.
81. Wang C, Liu T. Nori-based N, O, S, Cl co-doped carbon materials by chemical activation of $ZnCl_2$ for supercapacitor. *J Alloys Compd*. 2017;696:42-50.
82. Lin L, Xie H, Lei Y, Li R, Liu X, Ou J. Nitrogen source-mediated cocoon silk-derived N, O-doped porous carbons for high performance symmetric supercapacitor. *J Mater Sci Mater Electron*. 2020;31:10825-10835.
83. Shu Y, Bai Q, Fu G, et al. Hierarchical porous carbons from polysaccharides carboxymethyl cellulose, bacterial cellulose, and citric acid for supercapacitor. *Carbohydr Polym*. 2020;227:115346.
84. Hao X, Wang J, Ding B, et al. Bacterial-cellulose-derived interconnected meso-microporous carbon nanofiber networks as binder-free electrodes for high-performance supercapacitors. *J Power Sources*. 2017;352:34-41.
85. Shang Z, An X, Liu L, et al. Chitin nanofibers as versatile biotemplates of zeolitic imidazolate frameworks for N-doped hierarchically porous carbon electrodes for supercapacitor. *Carbohydr Polym*. 2021;251:117107.

How to cite this article: Taer E, Apriwandi A, Mardiah MA, Awitdrus, Taslim R. Synthesis free-template highly micro-mesoporous carbon nanosheet as electrode materials for boosting supercapacitor performances. *Int J Energy Res*. 2022;1-17. doi:10.1002/er.8493

Synthesis free-template highly micro-mesoporous carbon nanosheet as electrode materials for boosting supercapacitor performances

ORIGINALITY REPORT

15%	12%	10%	7%
SIMILARITY INDEX	INTERNET SOURCES	PUBLICATIONS	STUDENT PAPERS

PRIMARY SOURCES

1	acris.aalto.fi Internet Source	<1%
2	Archana Bansode, Mehul Barde, Osei Asafu-Adjaye, Vivek Patil et al. "Synthesis of Biobased Novolac Phenol–Formaldehyde Wood Adhesives from Biorefinery-Derived Lignocellulosic Biomass", ACS Sustainable Chemistry & Engineering, 2021 Publication	<1%
3	Lakshmana Kumar Bommineedi, Bidhan Pandit, Babasaheb R. Sankapal. "Spongy nano surface architecture of chemically grown BiVO4: High-capacitance retentive electrochemical supercapacitor", International Journal of Hydrogen Energy, 2021 Publication	<1%
4	www.tcsae.org Internet Source	<1%

5	Hui Chen, YaFei Hou, ZhiJie Wu, Peng Du, LaiHui Luo, WeiPing Li. "Simultaneous enhancement of discharge energy density and efficiency in the PMMA and PVDF blend films via introducing the Ni(OH)2 nanosheets", Journal of Alloys and Compounds, 2021 Publication	<1 %
6	Jishi Zhang, Mengchen Yang, Wenqian Zhao, Junchu Zhang, Lihua Zang. "Biohydrogen Production Amended with Nitrogen-Doped Biochar", Energy & Fuels, 2021 Publication	<1 %
7	Musen Zhou, Anthony Vassallo, Jianzhong Wu. " Data-Driven Approach to Understanding the Performance of Heteroatom-Doped Carbon Electrodes ", ACS Applied Energy Materials, 2020 Publication	<1 %
8	Lei Du, Gaixia Zhang, Xianhu Liu, Amir Hassanpour, Marc Dubois, Ana C. Tavares, Shuhui Sun. "Biomass‐derived nonprecious metal catalysts for oxygen reduction reaction: The demand‐oriented engineering of active sites and structures", Carbon Energy, 2020 Publication	<1 %
9	Muhamad Hafiz Hamsan, Norhana Abdul Halim, Siti Zulaikha Ngah Demon, Nurul Syahirah Nasuha Sa'aya et al. "SCOBY-based	<1 %

bacterial cellulose as free standing electrodes for safer, greener and cleaner energy storage technology", Heliyon, 2022
Publication

10	jddtonline.info Internet Source	<1 %
11	krclib.ncl.res.in Internet Source	<1 %
12	Amimul Ahsan. "Meet Our Editorial Board Member", Current Environmental Engineering, 2018 Publication	<1 %
13	Yao Li, Yeru Liang, Hang Hu, Hanwu Dong, Mingtao Zheng, Yong Xiao, Yingliang Liu. "KNO3-mediated synthesis of high-surface-area polyacrylonitrile-based carbon material for exceptional supercapacitors", Carbon, 2019 Publication	<1 %
14	vtechworks.lib.vt.edu Internet Source	<1 %
15	Antonio Wilson Macedo Carvalho Costa, Flavio Guerhardt, Silvestre Eduardo Rocha Ribeiro Júnior, Geovana Cânovas et al. "Biosorption of Cr(VI) using coconut fibers from agro-industrial waste magnetized using	<1 %

magnetite nanoparticles", Environmental Technology, 2020
Publication

16	Hanieh Shaki. "The use of electrospun nanofibers for absorption and separation of carbon dioxide: A review", Journal of Industrial Textiles, 2023 Publication	<1 %
17	Deepika, Manasvi Dixit, Hukum Singh, M. S. Attia, Mohammed A. Amin. "Recent innovations in properties of nanostructured glasses and composites", Journal of Experimental Nanoscience, 2021 Publication	<1 %
18	Submitted to Federal University of Technology Student Paper	<1 %
19	Jing Chen, Min Hong, Jiafu Chen, Tianzhao Hu, Qun Xu. "Fabrication of Hierarchical Porous Hollow Carbon Spheres with Few-layer Graphene Framework and High Electrochemical Activity for Supercapacitor", Applied Surface Science, 2018 Publication	<1 %
20	Submitted to National Institute of Technology, Rourkela Student Paper	<1 %

21	Submitted to University of Science and Technology Student Paper	<1%
22	core.ac.uk Internet Source	<1%
23	jmrt.com.br Internet Source	<1%
24	ruj.uj.edu.pl Internet Source	<1%
25	Submitted to Monash University Student Paper	<1%
26	biblio.cinvestav.mx Internet Source	<1%
27	esst.cip.com.cn Internet Source	<1%
28	journals.lww.com Internet Source	<1%
29	purehost.bath.ac.uk Internet Source	<1%
30	www.investigo.biblioteca.uvigo.es Internet Source	<1%
31	www.scribd.com Internet Source	<1%
32	Submitted to Istanbul Aydin University	

	Student Paper	<1%
33	kfi.ejournal.unri.ac.id Internet Source	<1%
34	www.wjgnet.com Internet Source	<1%
35	Mingquan Liu, Feng Wu, Lumin Zheng, Xin Feng, Ying Li, Yu Li, Ying Bai, Chuan Wu. " porous carbon monolith: Molecular cooperative enables sustainable production and capacitive energy storage ", InfoMat, 2021 Publication	<1%
36	era.library.ualberta.ca Internet Source	<1%
37	jbas.juw.edu.pk Internet Source	<1%
38	Submitted to Alfaisal University Student Paper	<1%
39	Masao Kitajima, Masamichi Sato, Hiroyuki Nishide. "Preparation of flat porous carbon films from paper-thin wood shavings and control of their mechanical, electrical and magnetic properties", Carbon, 2013 Publication	<1%
	ir.semi.ac.cn	

40	Internet Source	<1%
41	A G Elang Barruna, R Muhamad Naufal, Mohammad Ridho Nugraha, Iyan Subiyanto, Netti Tinaprilla, Achmad Subhan, Hudaya Chairul. "Material characteristics and electrochemical performance of lithium-ion capacitor with activated carbon cathode derived from sugarcane bagasse", IOP Conference Series: Earth and Environmental Science, 2021 Publication	<1%
42	Submitted to Indian Institute of Technology Jodhpur Student Paper	<1%
43	www.science.gov Internet Source	<1%
44	Submitted to University Der Es Salaam Student Paper	<1%
45	Submitted to Yeungnam University Student Paper	<1%
46	Submitted to University of Reading Student Paper	<1%
47	hal.archives-ouvertes.fr Internet Source	<1%
	repository.uin-suska.ac.id	

48	Internet Source	<1%
49	wjgnet.com Internet Source	<1%
50	Ana Claudia Pina, Nestor Tancredi, Conchi O. Ania, Alejandro Amaya. "Stabilisation of sheep wool fibres under air atmosphere: Study of physicochemical changes", Materials Science and Engineering: B, 2021 Publication	<1%
51	Submitted to Queen's University of Belfast Student Paper	<1%
52	Submitted to University of Birmingham Student Paper	<1%
53	ar.booksc.eu Internet Source	<1%
54	shi.buaa.edu.cn Internet Source	<1%
55	www.researchgate.net Internet Source	<1%
56	Submitted to American University in Cairo Student Paper	<1%
57	Submitted to Universiti Teknologi MARA Student Paper	<1%

58	Graziano Colombo, Emanuela Astori, Lucia Landoni, Maria L. Garavaglia et al. "Effects of the uremic toxin indoxyl sulphate on human microvascular endothelial cells", Journal of Applied Toxicology, 2022 Publication	<1 %
59	Submitted to Visvesvaraya National Institute of Technology Student Paper	<1 %
60	Submitted to Higher Education Commission Pakistan Student Paper	<1 %
61	Submitted to Queen Mary and Westfield College Student Paper	<1 %
62	Submitted to Swinburne University of Technology Student Paper	<1 %
63	Submitted to West De Pere High School Student Paper	<1 %
64	Yu-Chun Chiang, Wei-Ting Chin, Chih-Cheng Huang. "The Application of Hollow Carbon Nanofibers Prepared by Electrospinning to Carbon Dioxide Capture", Polymers, 2021 Publication	<1 %
65	profdoc.um.ac.ir Internet Source	<1 %

66	collections.lib.utah.edu Internet Source	<1%
67	p3m.poliban.ac.id Internet Source	<1%
68	doaj.org Internet Source	<1%
69	sejong.elsevierpure.com Internet Source	<1%
70	ueaeprints.uea.ac.uk Internet Source	<1%
71	Jia-Xing Jiang, Fabing Su, Abbie Trewin, Colin D. Wood et al. "Conjugated Microporous Poly(aryleneethynylene) Networks", Angewandte Chemie International Edition, 2007 Publication	<1%
72	Yujie Zhang, Honglei Chen, Shoujuan Wang, Xin Zhao, Fangong Kong. "Regulatory pore structure of biomass-based carbon for supercapacitor applications", Microporous and Mesoporous Materials, 2020 Publication	<1%
73	epub.uni-regensburg.de Internet Source	<1%
74	nottingham-repository.worktribe.com Internet Source	<1%

75	pdfcoffee.com Internet Source	<1 %
76	peerj.com Internet Source	<1 %
77	repository.ubaya.ac.id Internet Source	<1 %
78	Fan Jiang, Yahong Zhu, Zheng Liu, Xue Zhang, Wei Ma, Haitang Wu, Xiaohua Huang, Qiang Zhang. "Novel synthesis route for the preparation of mesoporous nitrogen-doped carbons from forestry wastes for supercapacitors", Surfaces and Interfaces, 2021 Publication	<1 %
79	beilstein-journals.org Internet Source	<1 %
80	edepot.wur.nl Internet Source	<1 %
81	res.mdpi.com Internet Source	<1 %
82	www.scirp.org Internet Source	<1 %
83	Junam Kim, Hoai Van T. Nguyen, Gyung Jin Bahk, Kyungwon Kwak, Kyung-Koo Lee. "Activated carbons effectively purified by	<1 %

post-heat treatment under vacuum conditions", Carbon Letters, 2021
Publication

84 Ma, Pei-Pei, Jie Du, Zhan-Bing He, Xiang-Ying Xing, and Tie-Zhen Ren. "Shape-controlled nanocrystal y-MnO2 : Preparation and electrochemical features : Shape-controlled nanocrystal y-MnO2 : Preparation and electrochemical features", physica status solidi (a), 2013. <1 %
Publication

85 Fuad Mustafanejad, Nooshin Sajjadi, Reza Marandi, Mojgan Zaeimdar. "Efficient removal of crystal violet by sulphonic-modified multi-walled carbon nano-tube and graphene oxide", Nanotechnology for Environmental Engineering, 2021 <1 %
Publication

86 Gabriela Durán-Jiménez, Emily T. Kostas, Lee A. Stevens, Will Meredith et al. "Green and simple approach for low-cost bioproducts preparation and CO2 capture", Chemosphere, 2021 <1 %
Publication

87 Jingge Ju, Nanping Deng, Dan Zhang, Jing Yan, Lei Li, Weimin Kang, Bowen Cheng. "Facile construction of PCNF&CNT composite material by one-step simultaneous <1 %

carbonization and chemical vapor deposition", Journal of Materials Science, 2018
Publication

Exclude quotes	Off	Exclude matches	Off
Exclude bibliography	Off		